International Journal Of
Industrial Electronics Control and Optimization
Print ISSN: 3517-2645
Online ISSN: 3568-2645
Homepage: https://ieco.usb.ac.ir/

Simplified and Accurate Predictive Control Method in Mono-Inverter Dual-Parallel Permanent Magnet Synchronous Motors

Mehdi Fadaie[1], Karim Abbaszadeh[2]✉, Alireza Siadatan[3]

Department of Electrical Engineering, Faculty of Electrical Engineering, Science and Research Branch, Islamic Azad University, Tehran, Iran.[1]
Department of Electrical Engineering, Faculty of Electrical Engineering K. N. Toosi University of Technology, Tehran, Iran.[2]
College of Technical and Engineering West Tehran Branch, Islamic Azad University, Tehran, Iran[3]
Corresponding author's email: abbaszadeh@kntu.ac.ir

Article Info

Article type:
Research Article

Article History:
Received 2022-01-06
Received in revised form 2022-04-10
Accepted 2022-05-26
Published online:2022-08-30

Keywords:
Inverter Dual Parallel,
Model Predictive Control,
PM Synchronous Motor.

ABSTRACT

Mono-Inverter Dual Parallel (MIDP) motors in transportation systems are the most effective method to manage energy consumption and reduce the volume, weight, and cost of electric motor drives. Unbalancing the load torques and changing the speed in unequal loading are the main problems in these systems. Hence, the latest methods of optimal control such as Model Predictive Control (MPC) have been proposed. However, these methods do not lead to accurate control of MIDP systems because the cost function is evaluated by the limited number of control signals or solved online after a long time-consuming. This paper deals with designing the current and speed controllers of the MIDP system through an effective MPC method in order to reduce the computing time of the control signals and improve the motor performance in any situation. Pontryagin's principle and the Lagrange method are used in designing the current and speed controllers respectively. These controllers constantly generate control signals as linear-parametric functions through the offline solving of the quadratic-linear cost function. After driving and simplifying the mathematical equations, the proposed method simulates. The simulation results of the proposed method are compared with the known Finite Control Set-Model Predictive Control (FCS-MPC) method in the MIDP motors. These results validate the prompt and accurate performance of the proposed controllers in transient and steady states.

I. Introduction

Attempt to control two motors fed by a single converter goes back to when researchers tried using an inverter for each wheelset and even for each bogie of the power trains. Subsequently, the Mono-Inverter Dual Parallel (MIDP) systems were introduced to be applied in high-inertia electrical locomotives with slow speed changes. The year 1977, namely [1], can be marked as the beginning of research in this field. When the MIDP system is used to drive two motors, only one inverter, rectifier, filter, DC link, and integrated controller are used, while it has to be used twice as much as all the devices used in typical drive methods. Controlling the motors in the MIDP systems, based on studies done, can be categorized into two groups which include the weighting-based control and the model-based control. There are two approaches to the weighting-based control. The first is the averaged vector control of motors [2]-[6]. There are some problems in this approach such as severe and lengthy fluctuations in the current waveforms, the dependence of the calculated commands on the motor type, and weak stability. Master-Slave (MS) is the second approach, in which the elimination of fluctuations and maintaining the stable performance of motors are the main concerns [7]-[9]. The method of reduced-order feedback linearization has been used on independent torque control in the MIDP system [10]. Although the designed controller could hardly control the system at singular points, it could drive the MIDP system under severe unequal load torques conditions. With the advent of powerful microcontrollers, the MPC

Copyright © 2022 Fadaei et al. by University of Sistan and Baluchestan. This work is licensed under a Creative Commons Attribution-Noncommercial 4.0 International license. (https://creativecommons.org/licenses/by-nc/4.0/). Non-commercial uses of the work are permitted, provided the original work is properly cited
DOI : 10.22111/IECO.2022.41196.1405

method was used to drive electrical motors.

Typically, there are two general approaches in executing the MPC methods for MIDP system control. The first approach is the Continues Control Set-Model Predictive Control (CCS-MPC) method [11]. It solves the cost function by using one of the optimal control methods and considering some limitations and system initial conditions. Therefore, it generates the control signals according to the model parameters, the initial condition of the control variables, and the state feedback values. Perhaps the pioneer of CCS-MPC is the Optimal Torque Predictive Control method [12], [13]. Severe fluctuations in the transient state and the tendency of the cost function to a non-zero value are among the problems in this research. The system constraints were used in [14] to determine control signals. However, the control loop of optimal angle displacement not only was prolonged the fluctuations of the control variables but also was increased the sensitivity of the method to the motor parameters.

The second approach, called Finite Control Set Model Predictive Control (FCS-MPC), was applied on two PMSM motors and two induction motors in [15] and [16], [17] respectively. If the electrical currents of the motors are defined as control variables in the cost function, the method is called Predictive Control Current (PCC). If the flux and torque are also defined as control variables in the cost function, the method is called Predictive Torque Control (PTC). This method is characterized by the simplicity of the design process, no need for voltage modulators, online optimization, and variable switching. Certainly, the lowest value of the cost function is not obtained by applying six control signals. Therefore, the Seek and Split Predictive Torque Control (SS-PTC) method used a large number of voltage space vectors is introduced [18]. Obviously, the obtained voltage vectors in the FCS-MPC method do not lead to the absolute minimum value of the cost function. As a result, further studies are needed to introduce a method to obtain optimal control signals for MIDP systems.

This paper presents a comprehensive analytical method for designing the current controller that can be used for most electrical motors in any structure. In addition, an effective speed controller is introduced based on the nominal power and the kinetic energy of the motors. Since the produced control signals in both controllers are linear-parametric functions from the state variables, the proposed drive technique saves significant computing time and processing memory. According to the design principles used in controllers, the proper performance of motors in the MIDP system is expected in both steady and transient states. The designed speed and current controllers, respectively based on the Lagrange method and the Pontryagin's Maximum Principle, are used to the cascade structure. The necessary and sufficient conditions are also considered for the controllability of the system at any given time.

This article is organized as follows. In the first part, the model of two PMSM motors will be obtained in a rotor reference frame. In the second part, the control signals are presented for both controllers, and the necessary and sufficient condition for generating control signals is examined. Then, in the MIDP system, the simulation results of the proposed method are compared with the FCS-MPC method. Finally, the conclusion is presented.

II. MIDP system drive structure

Fig. 1 shows the cascade structure of the MIDP system drive with PMSM motors. Instead of using the conventional proportional-integral controller in the outer loop, $\hat{I}_{qs}$ control signals are generated by the MPC method using the reference speed, the speed measured values and the estimated torque of both motors.

In the inner loop, the MPC method is employed to generate $\hat{V}_{qd}$ (voltage control signals) by measuring I_{qds} currents and motor speeds, and the space vector modulation method is used to produce inverter switching commands. In this configuration, the I_{ds} current commands in each motor are considered equal to zero, which maximizes the torque per ampere ratio in conditions that the load torques are equal.

A. Modelling of Two PMSM motors in MIDP system

In this paper, two identical surface-mounted PMSM motors are used in the MIDP system [19], whose electrical equations can be found in the rotor reference frame [20]. The rotor coordinates of the motors do not match when the mechanical load of the motors is not the same for a specific application or for a period of time. Since the inverter dq coordinate system cannot be matched to the coordinate system of both motors at any time, the electrical equations of the second motor are transferred to the rotor reference frame of the first one [21] as follows:

$$f_{dqs}^{r_1} = ({}^{r_2}K_s{}^{r_1}) f_{dqs2}^{r_2};$$
$${}^{r_2}K_s{}^{r_1} = \begin{bmatrix} \cos(\theta_{r1} - \theta_{r2}) & -\sin(\theta_{r1} - \theta_{r2}) \\ \sin(\theta_{r1} - \theta_{r2}) & \cos(\theta_{r1} - \theta_{r2}) \end{bmatrix} \quad (1)$$

where $f_{dqs2}^{r_2}$ is the state variable vectors of the second motor in its rotor reference frame, the transferred state variable vectors of the second motor to the rotor reference frame of the first motor is $f_{dqs2}^{r_1}$, and θ_{r1} and θ_{r2} are the electric angle displacements of motors, respectively. The electrical equations of the second motor in the dq coordinate system of the first motor are provided by Equ. (1) as follows:

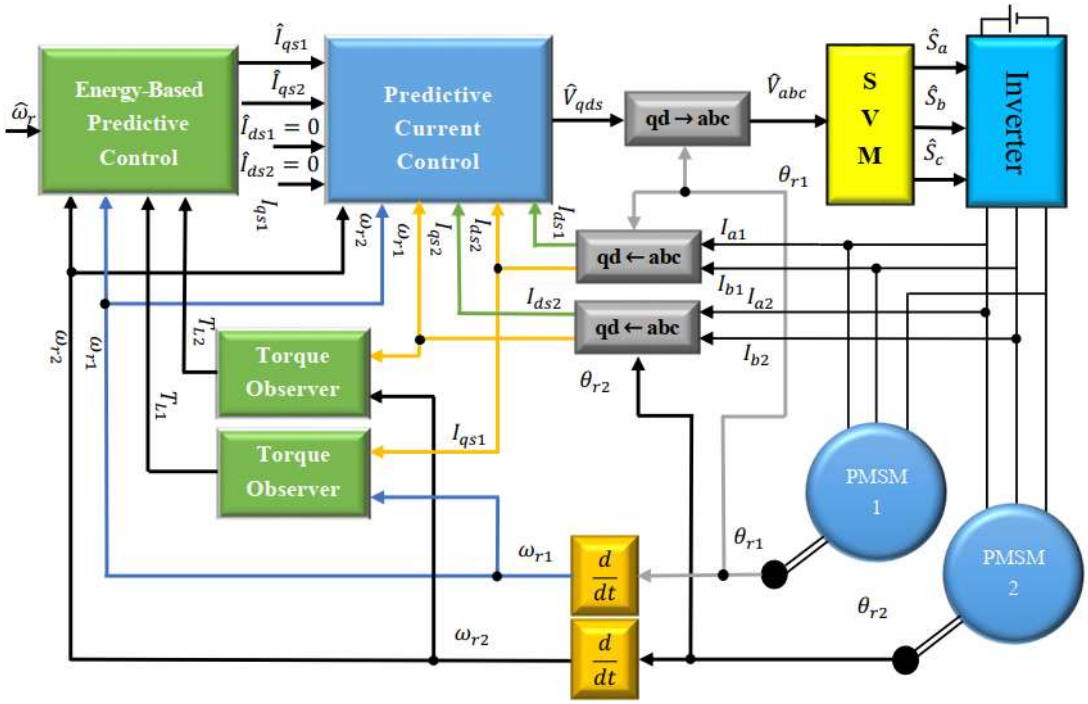


Fig. 1. Block diagram of the proposed method. The EPC block is related to speed control and the PCC block is related to current control.

$$\begin{cases} \frac{d}{dt}\left(I_{qs2}^{r_1}(t)\right) = \frac{1}{L}V_{qs2}^{r_1}(t) - \frac{r_s}{L}I_{qs2}^{r_1}(t) - \omega_{r1}(t)I_{ds2}^{r_1}(t) - \cdots \\ \qquad \ldots - \frac{1}{L}\omega_{r2}(t)\psi_f\cos(\theta'); \\ \frac{d}{dt}\left(I_{ds2}^{r_1}(t)\right) = \frac{1}{L}V_{ds2}^{r_1}(t) - \frac{r_s}{L}I_{ds2}^{r_1}(t) + \omega_{r1}(t)I_{qs2}^{r_1}(t) - \cdots \\ \qquad \ldots - \frac{1}{L}\omega_{r2}(t)\psi_f\sin(\theta'); \end{cases} \quad (2)$$

where $V_{qs}^{r_1}(t).I_{ds2}^{r_1}(t).I_{qs2}^{r_1}(t)$ and $V_{ds2}^{r_1}(t)$ are the stator current and voltage of the second motor in the first motor dq coordinate system.

III. Designing Controllers in MIDP system:

The control signal generation based on Pontryagin's Maximum Principle, employed in MPC-based current controller design, is described first.

A. Designing current controller based on Pontryagin's Maximum Principle:

The nonlinear model of the control system at t_i is defined by using Taylor expansion as:

$$\begin{cases} X^{\bullet}(t) = f(X(t).U(t).t) \cong A(X.t_i)X(t) + BU(t) + D(X.t_i); \\ X_{min} \le X(t) \le X_{max} \quad U_{min} \le U(t) \le U_{max} \end{cases} \quad (3)$$

In order to track the desired conditions by the controlled system, the performance index is considered as follows:

$$\mathcal{J} = Min\frac{1}{2}\Big[\left(X(t_f) - \hat{X}\right)^T Q_f\left(X(t_f) - \hat{X}\right) + \int_{t_i}^{t_f}\left(X(t) - \hat{X}\right)^T Q(X(t) - X^*) + U^T(t)RU(t)d\tau\Big]; \quad (4)$$

where $Q \ge 0$. $Q_f \ge 0$ and $R > 0$ are weighting matrices to be selected, $\hat{X}$ is the reference state vector, X is the optimal value of the state vector, t_f is the end of the predictive horizon, and $X(t_f)$ is the state vector at t_f. The first statement is the final cost function and the other is the integral cost function. Pontryagin's Maximization Principle can be used to solve the MPC problem [22]. For this purpose, the Pontryagin function is written as follows:

$$\mathcal{H} = Z\left(X(t).\hat{X}.t\right) + \psi^T(t)\left(f(X(t).U(t).t)\right); \quad (5)$$

where $\psi(t)$ is the quasi-variable state vector with equal dimension to the state vector $X(t)$, and $Z(X(t).X^*.t)$ is the second statement of Equ. (4). Based on the Pontryagin's Maximum Principle, the necessary optimization conditions are $X^{\bullet}(t) = \frac{\partial\mathcal{H}}{\partial\psi}$. $\psi^{\bullet}(t) = -\frac{\partial\mathcal{H}}{\partial X}$. and $\frac{\partial\mathcal{H}}{\partial U} = 0$, The linear equation of the controlled system and the necessary conditions of optimality make it possible to write the differential equations as follows:

$$\begin{cases} X^{\bullet}(t) = A\left(X(t_i)\right)X(t) - BU(t) + D(X(t_i).t_i); \\ \psi^{\bullet}(t) = -Q\left(X(t) - \hat{X}\right) - A^T\left(X(t_i)\right)\psi(t); \\ U(t) = R^{-1}B^T\psi(t); \\ X(t_i) = X_{t_i}; \\ \psi(t_f) = \left(\frac{\partial\left(X(t_f) - \hat{X}\right)^T Q_f\left(X(t_f) - \hat{X}\right)}{\partial X(t)}\right) = Q_f\left(X(t_f) - \hat{X}\right); \end{cases} \quad (6)$$

To calculate the control signals, the forward Euler method is used to approximate the left side of Equ. (6).

$$\frac{X(t_i+1) - X(t_i)}{\tau_p} = A\left(X(t_i)\right)X(t) - BR^{-1}B^T\psi(t) + D\left(X(t_i)\right); \quad (7)$$

$$\frac{\psi(t_i+1) - \psi(t_i)}{\tau_p} = -Q\left(X(t) - \hat{X}\right) - A^T\left(X(t_i)\right)\psi(t); \quad (8)$$

where τ_p is small enough. After simplifying the Equ. (7) and (8), calculating the predicted value of the state vector at the end

of the sampling interval, and also calculating the value of the quasi-state variable at the beginning of the sampling interval, $\psi(t_i)$ can be written as follows:

$$\psi(t_i) = \rho_1 M^{-1}\rho_2 X(t_i) + \rho_1\left((M^{-1}\rho_3\rho_1 - 1)\hat{X} + \tau_p M^{-1} D\right); \quad (9)$$

The calculations related to the coefficients $\rho_1.\rho_2.\rho_3$ and M can be found in the Appendix. By having $\psi(t_i)$. the control signals are obtained as follows:

$$\begin{cases} U(t_i) = \alpha\big(X(t_i)\big)X(t_i) + \beta\big(X(t_i)\big); \\ \alpha\big(X(t_i)\big) = -R^{-1}B^T\rho_1 M^{-1}\rho_2; \\ \beta\big(X(t_i)\big) = -R^{-1}B^T\rho_1\left((M^{-1}\rho_3\rho_1 - 1)\hat{X} + \tau_p M^{-1} D\right); \end{cases} \quad (10)$$

As can be seen in Equ. (10), the control signals are obtained as linear-parametric relations from the measurable state variables, which makes the time of online calculations shorter.

1) The reversibility matrix M:

The reversibility of matrix M in Equ. (10) should be reviewed because the controllability of the MIDP system depends on the M matrix reversibility. Otherwise, the proposed method would not be efficient. The M matrix can be written as follows:

$$M = \begin{bmatrix} m_{11}+1 & m_{12} & m_{13} & m_{14} \\ m_{21} & m_{22}+1 & m_{23} & m_{24} \\ m_{11} & m_{12} & m_{13}+1 & m_{14} \\ m_{21} & m_{22} & m_{23} & m_{24}+1 \end{bmatrix}$$

The coefficients $\rho_1.\rho_2.\rho_3$, and the M elements are provided in the Appendix. The weighting values should be $Q_{11} = Q_{33}.\ Q_{22} = Q_{44}.\ Q_{f11} = Q_{f33}$ and $Q_{f2} = Q_{f4}$ in the M matrix. Otherwise, there would be bias in motors. Reversibility is proven when the determinant of the M matrix is non-zero. Determinant of the M matrix is as follows:

$$Det(M) = 1 + \left(\frac{2Q_{11}}{R_{11}} + \frac{2Q_{22}}{R_{22}} + \frac{4Q_{11}Q_{22}}{R_{11}R_{22}}\left(\frac{\tau_p}{L}\right)^2\right)\left(\frac{\tau_p}{L}\right)^2 + \left(\frac{1}{\tau_p} - \frac{r_s}{L}\right)\left(\frac{2Q_{f11}}{R_{11}} + \frac{2Q_{f22}}{R_{22}} + \frac{4}{R_{11}R_{22}}\left(Q_{22}Q_{f11} + Q_{11}Q_{f22}\right)\left(\frac{\tau_p}{L}\right)^2 + \left(\frac{1}{\tau_p} - \frac{r_s}{L}\right)\frac{4Q_{f1}\ Q_{f22}}{R_{11}R_{22}}\left(\frac{\tau_p}{L}\right)^2\right)\left(\frac{\tau_p}{L}\right)^2; \quad (11)$$

When the statement of $\left(\frac{1}{\tau_p} - \frac{r_s}{L}\right)$ is chosen positively, the determinant of the M matrix will be non-zero. In the above approximation, it is assumed that the τ_p value is smaller than the electrical time constant of the motors. Thus, the M determinant is always non-zero.

B. MPC-based speed controller design

With the least fluctuation and in the shortest possible time, the motor speeds reach the reference speed when the designed speed controller adjusts the $\hat{I}_{qs}$ commands in the inner loop. Accordingly, the performance index is defined as follows:

$$\mathcal{J} = \min_{X}\left\{\frac{1}{2}\int_{t_i}^{t_f}\left(\hat{X} - X(t)\right)^T Q_{sw}(t)\left(\hat{X} - X(t)\right)d\tau\right\}; \quad (12)$$

where $X(t) = [\omega_{r_1}^{\bullet}(t) \quad \xi_{k_1}(t) \quad \omega_{r_2}^{\bullet}(t) \quad \xi_{k_2}(t)]^T$ is the state vector that contain the angular accelerations ($\omega_r^{\bullet}(t)$) and kinetic energies ($\xi_k(t)$). The element values of reference vector are $\left[0 \quad \frac{1}{2}J_t\left(\hat{\omega}_{r_1}(t)\right)^2 0 \quad \frac{1}{2}J_t\left(\hat{\omega}_{r_2}(t)\right)^2\right]^T$. The total inertia moment of the load and motor is J_t, and $Q_{sw}(t)$ is the deterministic positive weighting matrix. Since motors are not mechanically coupled (Fig. 1), therefore, the elements associated with their coupling will be zero in the $Q_{sw}(t)$ matrix. By replacing the state and reference vectors in the performance index and minimizing the integral cost function relative to the motor speed slopes, Equ. (13) is obtained.

$$\begin{cases} \omega_{r_1}^{\bullet}(t) = \frac{2J_t}{p^2}\left(\frac{Q_{sw_{12}}(t)+Q_{sw_{21}}(t)}{Q_{sw_{11}}}\right)\left(\left(\hat{\omega}_{r_1}\right)^2 - \left(\omega_{r_1}(t_i)\right)^2\right); \\ \omega_{r_2}^{\bullet}(t) = \frac{2J_t}{p^2}\left(\frac{Q_{sw_{34}}(t)+Q_{sw_{43}}(t)}{Q_{sw_{33}}}\right)\left(\left(\hat{\omega}_{r_2}\right)^2 - \left(\omega_{r_2}(t_i)\right)^2\right); \end{cases} \quad (13)$$

The reference and electrical angular speeds of the motors at t_i are $\hat{\omega}_{r_1}, \hat{\omega}_{r_2}, \omega_{r_1}(t_i), \omega_{r_2}(t_i)$, respectively.

By choosing $Q_{sw_{11}} = Q_{sw_{33}} = \frac{2}{p}\Delta t^2, Q_{sw_{12}}(t) = Q_{sw_{21}}(t) = \frac{1}{2T_{L_1}(t_i)}$ and also $Q_{sw_{34}}(t) = Q_{sw_{43}}(t) = \frac{1}{2T_{L_2}(t_i)}$ as well as by choosing an arbitrary value for $Q_{sw_{22}}$ and $Q_{sw_{44}}$, to keep the $Q_{sw}(t)$ matrix as deterministic positive, Equ. (13) is as follows:

$$\frac{2}{p}\omega_{r_k}^{\bullet}(t)T_{L_k}(t_i)\Delta t^2 = \frac{2J_t}{p^2}\left(\left(\hat{\omega}_{r_k}\right)^2 - \left(\omega_{r_k}(t_i)\right)^2\right); \quad (14)$$

where $T_{L_k}(t_i)$ is the load torque of the kth motor at t_i. Using the mechanical equation of PMSM motors [23], the $\hat{I}_{qs}$ commands are as follows:

$$\hat{I}_{qsk}^{r_1}(t_i) = \frac{8J.J_t}{\Delta t^2 3p\psi_f T_{L_k}(t_i)}\left(\left(\hat{\omega}_{r_k}\right)^2 - \left(\omega_{r_k}(t_i)\right)^2\right) + \frac{8B_m}{3p^2\psi_f}\omega_{r_k}(t_i) + \frac{4}{3p\psi_f}T_{L_k}(t_i); \quad (15)$$

where k = 1, 2. Since the balance between the required energy and the kinetic energy on the motor shaft plays an important role in the generation of the control signals, this method of speed control can be introduced as Energy-based Predictive Control (EPC). When the speed variation of each motor causes the obtained commands by Equ. (15) to exceed the nominal current limits, the rated current value of the motors must replace with them.

1) Load torque calculation

Since Equ. (15) is dependent on the load torque, T_L needs to be available to set the $\hat{I}_{qs}^{r_1}$ command values. The load torque is usually measured by a torque meter or is calculated using estimation methods. Since a torque meter increases the cost and the measurement noise of electric propulsion, computational methods are used to estimate the amount of load torque. Considering the mechanical equation and the electromagnetic torque equation of the surface-mounted PMSM motor, the load

torque equation can be written, using the backward Euler approximation, as follows:

$$T_L(t_i) = \frac{3}{2}\frac{p}{2}\psi_f I_{qs}^r(t_i) - J\frac{2}{p}\left(\frac{\omega_r(t_i)-\omega_r(t_{i-1})}{\tau_p}\right) - B_m\frac{2}{p}\omega_r(t_i); \quad (16)$$

The value of load torque is set equal to the average of the last 10 samples to increase the accuracy of the calculated value.

IV. Simulation results

The performance and capability of the proposed controller are evaluated by MATLAB/Simulink software. Because low-inertia motors have fast dynamics, selecting such a motor can be a major challenge for controllers to generate control signals. Since the controller performance was very good in low inertia motors, the proper performance is not far from expectation in high inertia motors. Hence, two identical PMSM motors manufactured by LS Company with XML-SB04A series are chosen as MIDP system motors. The specifications are listed in Table 1. The specifications of the used SVM modulation inverter are listed in Table 2. According to Section 3, there are parameters in the internal and external loop controllers whose values must be specified.

TABLE 1
PMSM MOTOR PARAMETERS.

Motor Parameter		Parameter Value
Nominal Power	P_{rate}	400^{Watt}
Nominal Current	I_{rate}	2.89^{A}
Poles Number	p	8
Stator Resistance	r_s	0.82^{Ω}
Stator Inductance	L	3.66^{mH}
Magnet Flux	ψ_f	0.0734^{Wb}
Nominal Speed	N_{syn}	$3000^{r.p.m}$
Nominal Torque	T_{rate}	$1.27^{N.m}$
Maximum Torque	T_{max}	$3.82^{N.m}$
Moment of Inertia	J	0.0321×10^{-4} Kg.m.m
Friction Coefficient	B_m	0.6×10^{-6} N.m.Sec

TABLE 2
THREE-PHASE INVERTER PARAMETERS

Inverter Parameter		Parameter Value
DC Power Supply	E_{DC}	173^{V}
Switching Frequency	f_{SW}	8^{KHz}
On-Mode Resistance	$R_{DS(on)}$	0.019^{Ω}

The τ_p value is preferred 0.125×10^{-3} and the weighting matrices in the design of the inner loop controller is selected as fallows:

$$Q_f = \begin{bmatrix} 280 & 0 & 0 & 0 \\ 0 & 5800 & 0 & 0 \\ 0 & 0 & 280 & 0 \\ 0 & 0 & 0 & 5800 \end{bmatrix}; Q = \begin{bmatrix} 15 & 0 & 0 & 0 \\ 0 & 85 & 0 & 0 \\ 0 & 0 & 15 & 0 \\ 0 & 0 & 0 & 85 \end{bmatrix};$$

Also, the elements of the R weighting matrix are equals to one. Based on Table 1 and the mentioned weighting matrices, Equ. (10) can be obtained as written in the footnote. In the EPC speed controller, $\Delta t = 0.0118$. The sampling frequency of the current feedback signals is assumed to be 10^{KHz}.

A. Comparing the Proposed Method performance with the FCS-MPC:

The FCS-MPC method as an efficient approach has been used in the MIDP motors. The outer loop control signals of the FCS-MPC method are generated via conventional PI controllers. On the other hand, the inner loop control signals are selected among six voltage vectors which are resulted in the lowest value of the cost function.

The cost function is defined as follows:

$$CF = Min\sum_{j=1}^{2}\left[K_{\psi_j}\left|\hat{I}_{ds_j} - I_{ds_j}^{r_1}\right|^2 + K_{T_j}\left|\hat{I}_{qs_j} - I_{qs_j}^{r_1}\right|^2\right]; \quad (18)$$

where $\hat{I}_{dqs}$ are the reference control signals generated by the outer controller, and $I_{dqs}^{r_1}$ are obtained by discretizing Equ. (2). The constant coefficients are $K_{\psi_j} = 0.01$ and $K_{T_j} = 0.110$.

In what follows, the FCS-MPC performance, which has rapid in generating control signals, and the proposed method are compared in three different control modes.

$$\begin{bmatrix} V_{qs}^{r_1} \\ V_{ds}^{r_1} \end{bmatrix} = \alpha(X(t_i))\begin{bmatrix} I_{qds_1}^{r_1} \\ I_{qds_2}^{r_1} \end{bmatrix} + \beta^{(1)}(X(t_i))\begin{bmatrix} \hat{I}_{qds_1}^{r_1} \\ \hat{I}_{qds_2}^{r_1} \end{bmatrix} - \beta^{(2)}(X(t_i))\left(\frac{\psi_f}{L}\right)\left[\omega_{r_1} \quad 0 \quad \omega_{r_2}\cos(\theta_{r_1}-\theta_{r_2}) \quad \omega_{r_2}\sin(\theta_{r_1}-\theta_{r_2})\right]^T;$$

$$\alpha(X(t_i)) = \begin{bmatrix} -14.2328\left(\frac{\omega_{r_1}^2+k_{c1}}{\omega_{r_1}^2+k_{c5}}\right) & 0.0018\omega_{r_1}\left(\frac{\omega_{r_1}^2+k_{c1}}{\omega_{r_1}^2+k_{c5}}\right) & -14.2328\left(\frac{\omega_{r_1}^2+k_{c1}}{\omega_{r_1}^2+k_{c5}}\right) & 0.0018\omega_{r_1}\left(\frac{\omega_{r_1}^2+k_{c1}}{\omega_{r_1}^2+k_{c5}}\right) \\ -0.0018\omega_{r_1}\left(\frac{\omega_{r_1}^2+k_{c2}}{\omega_{r_1}^2+k_{c5}}\right) & -14.2301\left(\frac{\omega_{r_1}^2+k_{c2}}{\omega_{r_1}^2+k_{c5}}\right) & -0.0018\omega_{r_1}\left(\frac{\omega_{r_1}^2+k_{c2}}{\omega_{r_1}^2+k_{c5}}\right) & -14.2301\left(\frac{\omega_{r_1}^2+k_{c2}}{\omega_{r_1}^2+k_{c5}}\right) \end{bmatrix};$$

$$\beta^{(1)}(X(t_i)) = \begin{bmatrix} 14.64\left(\frac{\omega_{r_1}^2+k_{c3}}{\omega_{r_1}^2+k_{c5}}\right) & 22.4128\left(\frac{\omega_{r_1}}{\omega_{r_1}^2+k_{c5}}\right) & 14.64\left(\frac{\omega_{r_1}^2+k_{c3}}{\omega_{r_1}^2+k_{c5}}\right) & 22.4128\left(\frac{\omega_{r_1}}{\omega_{r_1}^2+k_{c5}}\right) \\ -1.0820\left(\frac{\omega_{r_1}}{\omega_{r_1}^2+k_{c5}}\right) & 14.64\left(\frac{\omega_{r_1}^2+k_{c4}}{\omega_{r_1}^2+k_{c5}}\right) & -1.0820\left(\frac{\omega_{r_1}}{\omega_{r_1}^2+k_{c5}}\right) & 14.64\left(\frac{\omega_{r_1}^2+k_{c4}}{\omega_{r_1}^2+k_{c5}}\right) \end{bmatrix};$$

$$\beta^{(2)}(X(t_i)) = \frac{1}{\omega_{r_1}^2+k_{c5}}\begin{bmatrix} -0.0018(\omega_{r_1}^2+k_{c3}) & -0.0028\omega_{r_1} & -0.0018(\omega_{r_1}^2+k_{c3}) & -0.0028\omega_{r_1} \\ 1.3525\times10^{-4}\omega_{r_1} & 0.0018(\omega_{r_1}^2+k_{c4}) & 1.3525\times10^{-4}\omega_{r_1} & 0.0018(\omega_{r_1}^2+k_{c4}) \end{bmatrix};$$

$$k_{c1} = 60.455\times10^6;\ k_{c2} = 60.477\times10^6;\ k_{c3} = 60.467\times10^6;\ k_{c4} = 60.478\times10^6;\ k_{c5} = 60.479\times10^6;$$

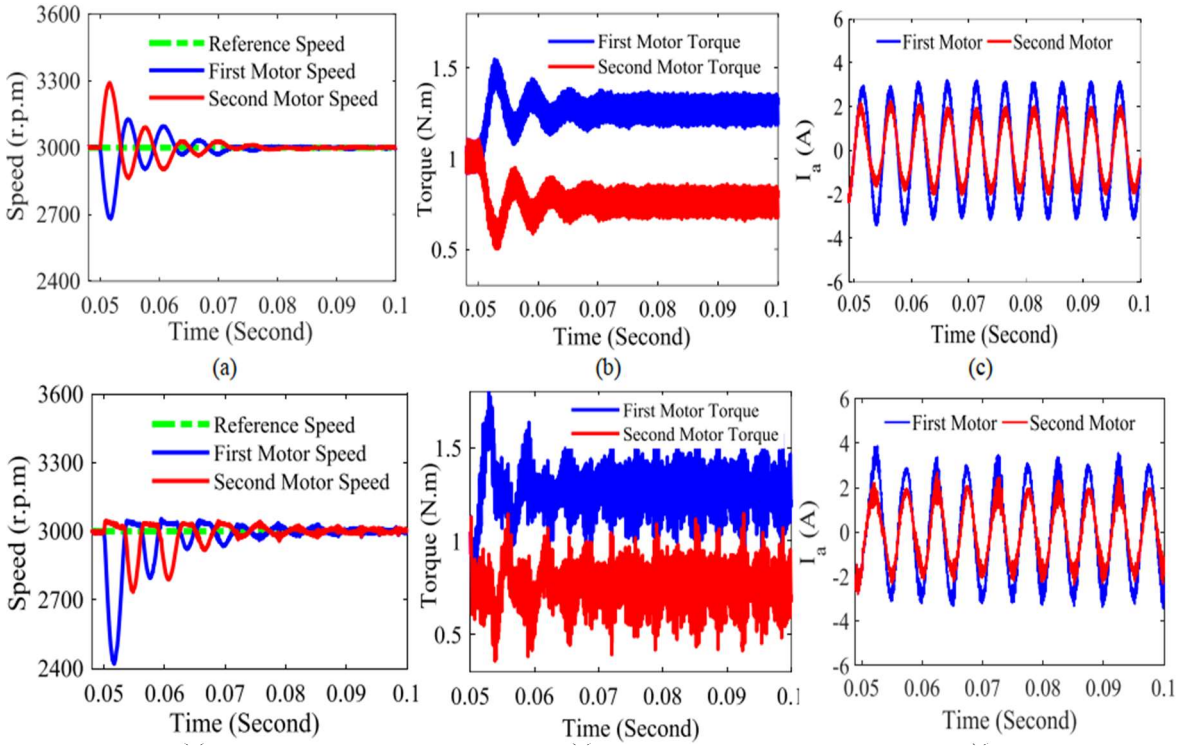


Fig. 2. The waveforms of the speed, torque, and current in the first strategy. (a)-(c) The waveforms in proposed method. (d)-(f) The waveforms in FCS-MPC method.

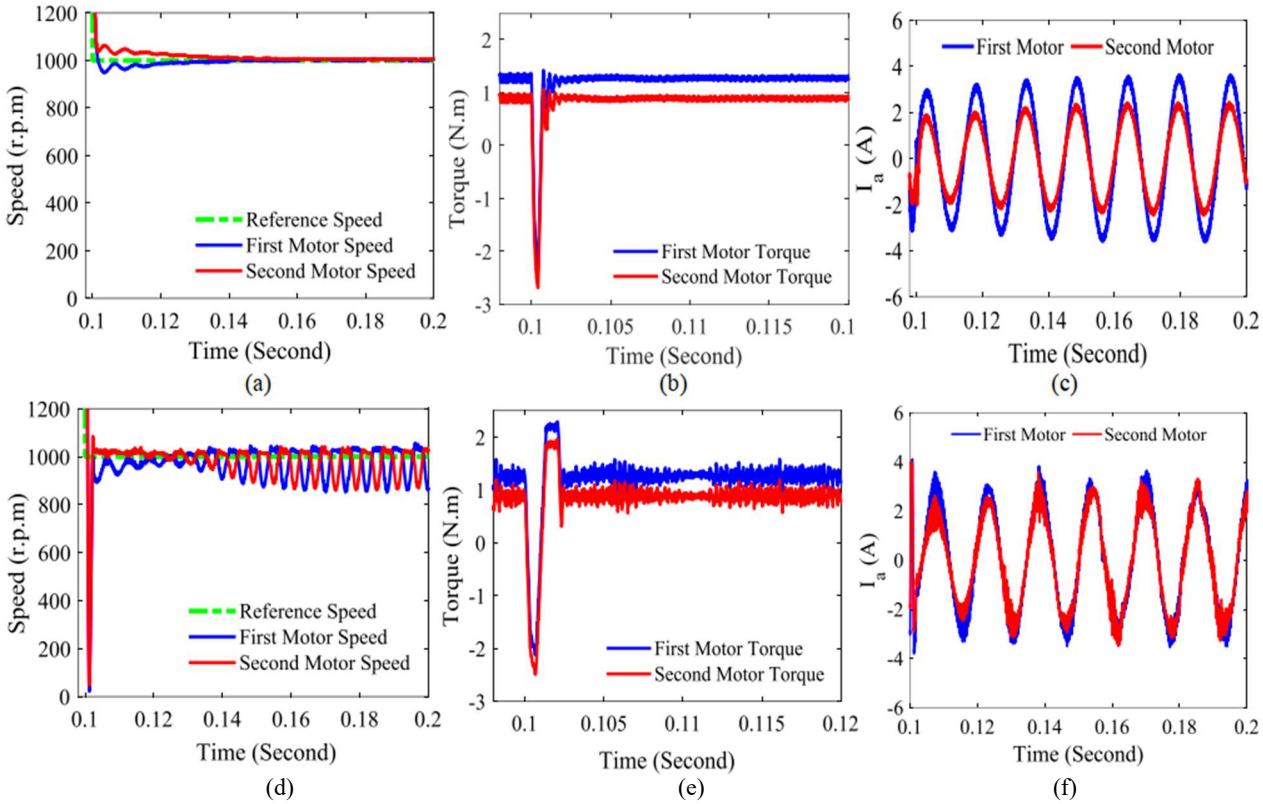


Fig. 3. The waveforms of the speed, torque, and current in the second strategy. (a)-(c) The waveforms in proposed method. (d)-(f)

1) Torque Unbalance at rated speed:

In this stage, both motors are rotating with $3000^{r.p.m}$, and their load torques are equal to $0.8^{P.U}$. In 0.05 seconds, the load torque of the motors is abruptly changed so that $T_{L1} = 1.0^{P.U}$ and $T_{L2} = 0.6^{P.U}$. The results obtained in this strategy are

shown in Fig. 2. Both methods could greatly handle the unbalance conditions, and the MIDP motors arrived in a steady state. However, the transient state performance of the proposed method has been better than the FCS-MPC method. If one compares the speed waveforms illustrated in Fig. 2(a) and 2(d), the severe undershoot that occurred in the first period is significant in the first motor speed.

As a result, the FCS-MPC method has not been able to have simultaneous control over both motors. Considering the Integral Square Error (ISE) of the speed waveforms reveals the performance of both methods in steady-state. The ISE is obtained by the following equation:

$$ISE = \sum_{k=1}^{2}\left(\hat{\omega}_{r,k} - \omega_{r,k}\right)^2 \Delta t; \quad (19)$$

Table 3 shows the ISE of the speeds at rated speed command and different load torque conditions. It shows that the steady-state performance of the designed controller, compared with the FCS-MPC method, has less distortion at nominal speed.

TABLE 3
COMPARISON OF ISE.

Speed	Load Torque	Motor No	ISE	
			Proposed MPC	FCS-MPC
3000	$T_{L2}=T_{L1}$	M_1	0.0179	0.2449
		M_2	0.0179	0.2449
	$T_{L2}=\%70T_{L1}$	M_1	0.0504	0.2560
		M_2	0.0311	0.2563

The presence of ripple in the torque waveforms (Fig. 2(e)) is another problem that is far less in the proposed method (Fig. 2(b)), although a sentence is not included in the cost function of the proposed method to reduce ripple. Comparing Fig. 2(c) and 2(f), no fluctuation is observed in the phase 'a' current of both motors. However, there is no disturbance in the phase 'a' currents of the proposed method, while some disturbances can be seen in the current peaks that cause increasing the switching losses. It should be noted that the angle difference between phase 'a' currents is observed in both methods due to the unbalance of torques. Indeed, the load torque of the second motor is less than the first motor, and the currents of the second motor will be ahead of the first motor.

2) Changing in speed command at unequal load torques:

This strategy occurs in 0.1 seconds, and the speed command is reduced from $3000^{r.p.m}$ to $1000^{r.p.m}$, while the load torque of motors is $T_{L1} = 1.0^{P.U}$ and $T_{L2} = 0.7^{P.U}$, respectively. This strategy aims to challenge both methods in managing excess energy. The braking torque is used to decelerate the motor speed. In a transient state, the speed of both motors in the proposed method has arrived at the new speed command without overshoot or undershoot (Fig. 3(a)). After applying the braking torque, the torques have also returned at previous values without significant fluctuation (Fig. 3(b)). However, the speed of the motors in the FCS-MPC method has deviated from the new speed command by about 1000 rpm (Fig. 3(d)), and the torques have had an overshoot during the same period (Fig. 3(e)).

Regarding the dynamic performance of the FCS-MPC controllers within the interval, the transient state fluctuations can be attributed to the excess energy imposed on motors.

However, in the proposed method, the new reference speed value is taken into account in the prediction horizon of the external loop controller. Therefore, from the very beginning, it applies the required braking torque to the motors, and the amount of braking torque decreases as the motor speeds approach the reference value.

Consequently, no excess energy is applied to two motor shafts. By comparing 3(a) and 3(d) in a steady-state, the speeds have constant fluctuation of nearly 200 r.p.m in the FCS-MPC method, while the motors in another method have tracked exactly the new speed command.

3) Changing the rotation direction at equal load torques

This strategy deals with the issue of changing the rotation direction of the motors form $3000^{r.p.m}$ to $-3000^{r.p.m}$, while the load torques are in the rated values. As can be seen, both methods could be able to track the new speed command. However, the FCS-MPC method has a fluctuation in the speed and torque waveforms (Fig. 4(c) and 4(d)), while the proposed method does not fluctuate in the waveforms (Fig. 4(a) and 4(b)). Fig. 4(e) compares the performance of both methods by the cost function presented in Equ. (18). Obviously, the proposed method could be able to control the MIDP motors optimal in transient and steady states.

B. Comparing the Computation Time of the Inner Loop Control Signals in Two Methods:

Table 4 shows the execution time of the current controller in the FCS-MPC and proposed methods in a sampling interval. The tic-toc command is used in MATLAB 2018b to measure the computation time. The system executing the software has an Intel Corei7-3610QM processor with a frequency of 2.3 GHz.

TABLE 4
ELAPSED TİME TO PRODUCE CONTROL SİGNALS.

	Proposed MPC	FCS-MPC
Elapsed time	0.007535^{ms}	0.013147^{ms}

The results indicate that when the MIDP system is driven using the proposed MPC method, it is approximately 1.745 times less time-consuming than the FCS-MPC method. The time saved frees microcontroller capacity to perform position and

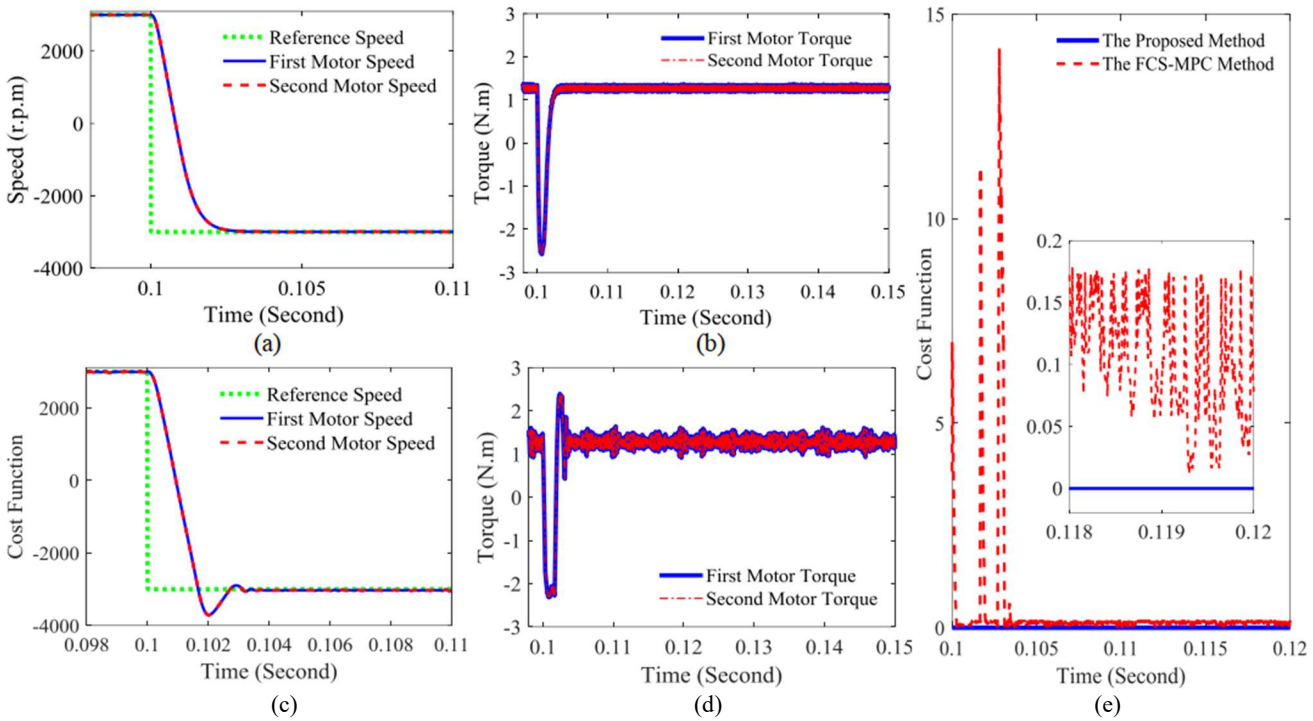


Fig. 4. The waveforms of the speed, torque, and cost function in the third strategy. (a)-(b) The waveforms in proposed method. (c)-(d) The waveforms in FCS-MPC method. (e) The cost function in both methods

speed sensorless control.

V. CONCLUSIONS

This paper has presented a cascade structure for driving two parallel synchronous motors powered by a three-phase inverter. The outer loop controller is designed based on optimizing the motors' energy. Its control signals, the electric currents of motors, are presented as analytical functions of control variables and feedback signals. This loop adjusts the speed slope of the motors so that both the excess energy is not imposed on the motors and the speed of the motors reaches speed command in the steady-state. On the other hand, the current controller design in the inner loop is based on the Pontryagin maximum principle. The used method has led to the accurate tracking of the outer loop current commands. The current ripple has also decreased compared to the conventional FCS-MPC method. Therefore, reducing the inverter switching losses in the proposed method is not unexpected. Another feature of the proposed method is the significant reduction in computational volume that has been caused a reduction in the required time to generate control signals. Since the control signals in both controllers are presented as analytical functions, most of the calculations are performed offline. Due to the agility of the controllers, the processing time of the calculations for generating control signals has significantly reduced. As a result, an inexpensive microcontroller can be used that executes a small number of instructions per sample time. It also frees up microcontroller capacity to perform observer calculations in sensorless controls. The results confirm that the proposed method could generate the control signals that ultimately are led to the realization of the minimum cost function. According to obtain results, in MIDP systems, the overall performance of the designed controllers has been far better than most of the model-based control methods.

VI. Appendix

The coefficients $\rho_1, \rho_2, \rho_3, \rho_4$ and M elements are as follows:

$$\rho_1 = [\rho_4 Q_f + Q\tau_p]; \quad \rho_2 = (I + A(X(t_i))\tau_p);$$

$$\rho_3 = BR^{-1}B^T\tau_p; \ \rho_4 = (I + A^T(X(t_i))\tau_p);$$

$$M = I + \rho_3\rho_1; \ \ m_{ii} = \left(\frac{\tau_p}{L}\right)^2\left(\frac{Q_{ii}}{R_{ii}} + \frac{Q_{fii}}{R_{ii}}\left(\frac{1}{\tau_p} - \frac{r_s}{L}\right)\right); \ \ i = 1.2$$

$$m_{ik} = \left(\frac{\tau_p}{L}\right)^2\left(\frac{Q_{kk}}{R_{ii}} + \frac{Q_{kk}}{R_{ii}}\left(\frac{1}{\tau_p} - \frac{r_s}{L}\right)\right); \ k = 3.4,$$

$$m_{ik} = \left(\frac{\tau_p}{L}\right)^2\frac{Q_{fjj}}{R_{ii}}\omega_{r1}(t_i); \quad j = 2.3.4,$$

REFERENCES

[1] A. Plunkett and D. Plette, "Inverter-induction motor drive for transit cars," IEEE Transactions on Industry Applications, no. 1, pp. 26-37, 1977.

[2] J. M. Lazi, Z. Ibrahim, M. H. N. Talib, and R. Mustafa, "Dual motor drives for PMSM using average phase current technique," in 2010 IEEE International Conference on Power and Energy, 2010: IEEE, pp. 786-790.

[3] J. M. Lazi, Z. Ibrahim, and M. Sulaiman, "Mean and diffrential torque control using hysteresis current controller for dual PMSM drives," in Journal of Theoretical and Applied information Technology, 2011: Citeseer.
[4] G. Brando, L. Piegari, and I. Spina, "Simplified optimum control method for monoinverter dual parallel PMSM drive," IEEE Transactions on Industrial Electronics, vol. 65, no. 5, pp. 3763-3771, 2017.
[5] Z. I. Jurifa Mt Lazi, Md Hairul Nizam Talib, Auzani Jidin, "Non-independent speed control for dual-PMSM drives fed by a single three-leg VSI," vol. 20, pp. 1717-1724, 3 December 2020, doi: 10.11591/ijeecs.v20.i3.pp1717-1724.
[6] F. Xu, L. Shi, and Y. Li, "The weighted vector control of speed-irrelevant dual induction motors fed by the single inverter," IEEE transactions on power electronics, vol. 28, no. 12, pp. 5665-5672, 2013.
[7] M. Ebadpour, M. B. B. Sharifian, and E. Babaei, "Modeling and control of dual parallel BLDC motor drive system with single inverter," in 2017 International Electrical Engineering Congress (iEECON), 2017: IEEE, pp. 1-4.
[8] T. Liu and M. FADEL, "A controller proposed for mono-inverter multiple-PMSM system," in Proc. 20th IFAC World Congr., 2017, vol. 50: Elsevier, pp. 14800-14805.
[9] T. Liu and M. Fadel, "An efficiency-optimal control method for mono-inverter dual-PMSM systems," IEEE Transactions on Industry Applications, vol. 54, no. 2, pp. 1737-1745, 2017.
[10] T. Liu, X. Ma, F. Zhu, and M. Fadel, "Reduced-Order Feedback Linearization for Independent Torque Control of a Dual Parallel-PMSM System," IEEE Access, vol. 9, pp. 27405-27415, 2021.
[11] N. L. Nguyen, M. Fadel, and A. Llor, "Predictive Torque Control-A solution for mono inverter-dual parallel PMSM system," in 2011 IEEE International Symposium on Industrial Electronics, 2011: IEEE, pp. 697-702.
[12] Š. Janouš, J. Talla, Z. Peroutka, and V. Šmídl, "Predictive Control of Parallel Induction Motors Fed by Single Inverter with Common Current Sensors," in IECON 2018-44th Annual Conference of the IEEE Industrial Electronics Society, 2018: IEEE, pp. 5843-5848.
[13] M. A. Abbasi and A. R. B. HUSAIN, "Model predictive control of a dual induction motor drive fed by a single voltage source inverter," Turkish Journal of Electrical Engineering & Computer Sciences, vol. 26, no. 3, pp. 1623-1637, 2018.
[14] N. L. Nguyen, M. Fadel, and A. Llor, "A new approach to predictive torque control with dual parallel PMSM system," in 2013 IEEE International Conference on Industrial Technology (ICIT), 2013: IEEE, pp. 1806-1811.
[15] G. Cimini, D. Bernardini, A. Bemporad, and S. Levijoki, "Online model predictive torque control for permanent magnet synchronous motors," in 2015 IEEE International Conference on Industrial Technology (ICIT), 2015: IEEE, pp. 2308-2313.
[16] A. BOUARFA and M. FADEL, "Optimal predictive torque control of two PMSM supplied in parallel on a single inverter," IFAC-PapersOnLine, vol. 48, no. 30, pp. 84-89, 2015.
[17] T. Liu and M. Fadel, "Performance comparison of control strategies for mono-inverter dual-PMSM system," in 2016 IEEE International Power Electronics and Motion Control Conference (PEMC), 2016: IEEE, pp. 637-642.
[18] A. Cervone, L. Di Noia, R. Rizzo, I. Spina, and R. Miceli, "A Constrained Optimal Model Predictive Control for Mono Inverter Dual Parallel PMSM Drives," in 2018 7th International Conference on Renewable Energy Research and Applications (ICRERA), 2018: IEEE, pp. 1501-1507.
[19] A. HossienPour and A. Khajeh, "Determining Optimal Value of Pole Arc to Pole Pitch Ratio in order to Increasing Average Torque and Decreasing Unbalance Magnetic Force in Hybrid Electrical Vehicle," International Journal of Industrial Electronics Control and Optimization, vol. 4, no. 4, pp. 445-451, 2021.
[20] K. Koiwa, T. Kuribayashi, T. Zanma, K.-Z. Liu, and M. Wakaiki, "Optimal current control for PMSM considering inverter output voltage limit: model predictive control and pulse-width modulation," IET Electric Power Applications, vol. 13, no. 12, pp. 2044-2051, 2019.
[21] H. Wan, Y. Pan, and J. Huang, "Comparative Study of VC and DTC for Single-Inverter Dual-Motor System," International Journal of Digital Content Technology and its Applications, vol. 6, no. 18, p. 587, 2012.
[22] N. Tauchnitz, "The Pontryagin maximum principle for nonlinear optimal control problems with infinite horizon," Journal of Optimization Theory and Applications, vol. 167, no. 1, pp. 27-48, 2015.
[23] K. Akbari, B. Rezaie, and S. Khari, "Designing full-order sliding mode controller based on ANFIS approximator for uncertain nonlinear chaotic systems," International Journal of Industrial Electronics, Control and Optimization, vol. 2, no. 1, pp. 39-46, 2019.



Mehdi Fadaie received the M.S. degree in Electrical Engineering from the K. N Toosi University of Technology, Tehran, Iran, in 2010. He has been working toward the Ph.D. degree in electrical machines and drives in Department of Electrical Engineering of the Science and Research Branch, Azad University, Tehran, Iran. His thesis concerned model predictive control, permanent-magnet synchronous machines, voltage-source inverters, and mono-inverter dual-parallel motors. His main research activity concerns in research on advanced control techniques for motor drives and motion control and variable-speed applications. He is currently a faculty member of Islamic Azad University, Bojnourd.



Karim Abbaszadeh, received the B.S. degree in communication engineering from K. N. Toosi University of Technology, Tehran, Iran, in 1991, and the M.S. and Ph.D. degrees in electrical engineering from Amir Kabir University of Technology, Tehran, Iran, in 1997 and 2000, respectively, From 2001 to 2003. He was a Research Assistant with the Department of Electrical Engineering, Texas A&M University, and College Station, TX, USA. He became an Assistant Professor in 2002, an Associate Professor in 2007, and a Full Professor of power electronics and electrical machine and drives in 2012; He is currently a full Professor with the Department of Electrical Engineering, K. N. Toosi University of Technology. His current research interests include power electronics and its applications such as in wind turbines, PV systems, electric machinery, and variable-speed drives. He has published more than 100 journal papers in the fields of power electronics and its applications. He is the author of two books in power electronics and its applications. . He is actively involved in presenting short courses and consulting in his area of expertise to various industries.



Alireza Siadatan (S'07, M'13, SM'18) received the B.Sc., Ph.D. and Postdoc degrees in electrical engineering from Shahid Beheshti University G.C., Tehran, IRAN, in 2002, 2013 and 2014, respectively, and the M.Sc. degree in electrical engineering from Azad University, south Tehran branch. He was a Visiting Student in Wisconsin University at Madison, 2012, USA. He has published around 170 Journal and conference papers and 15 patents. He joined the Azad University, West Tehran Branch, Iran, in 2008. Currently, He is a Visiting Professor at University of Toronto, CANADA. His current research interests include electric machines design and drives, BCI, renewable energy, special machines such as SRM, SynRM and power electronics.